Supplement of Atmos. Chem. Phys., 24, 2365–2376, 2024
https://doi.org/10.5194/acp-24-2365-2024-supplement

Atmospheric Chemistry and Physics
Open Access
EGU

Supplement of

Frequent haze events associated with transport and stagnation over the corridor between the North China Plain and Yangtze River Delta

Feifan Yan et al.

Correspondence to: Yang Gao (yanggao@ouc.edu.cn)

This supplemental information includes 3 tables and 7 figures.

Table captions

Table S1 Model configuration of WRF.

Table S2 The evaluation of daily meteorological parameters, including air temperature at 2 m (T_2), specific humidity at 2 m (Q_2), wind speed (WS_{10}), and direction (WD_{10}) at 10 m from WRF model simulation and NCDC observation.

Table S3 The total number of polluted days exceedance in SWLY during winters in 2014-2019.

Figure Captions

Fig. S1 The simulation domains of WRF (black square), CMAQ (magenta square) and the regions of NCP (red square), SWLY (green square), and YRD (blue square) used for the analysis.

Fig. S2 Scatter plot of simulated and observational daily mean $PM_{2.5}$ over three regions (NCP, SWLY, and YRD) from 2014 to 2019. The linear regression is marked in red line. The statistical parameters are also shown on the top left, including mean fractional bias (MFB), mean fractional error percent (MFE), and correlation coefficient (R), with the asterisk on the top left of R indicating statistical significance ($P < 0.05$).

Fig. S3 The cumulative distribution function of observational daily $PM_{2.5}$ in wintertime of SWLY in 2014-2019. The grey, green and orange dotted lines implies 75, 150, and 250 μg m^{-3} of $PM_{2.5}$ concentrations, respectively.

Fig. S4 The regional mean total frequency (a) and duration (b) of observational $PM_{2.5}$ for three categories (I: 75-150 μg m^{-3} II: 150-250 μg m^{-3}, III: greater than 250 μg m^{-3}) over SWLY, NCP and YRD in winter during 2014-2019.

Fig. S5 (a)-(c): Monthly average emissions of (t/month) from MEIC emission inventory in winter 2016; (d) The monthly average emissions of $PM_{2.5}$, NO_X, and SO_2 derived from MEIC in SWLY and NCP in winter 2016.

Fig. S6 Trajectories from FLEXPART-WRF in YRD for episodes of Type I, with different colors indicating the number of hours prior to the end of the event (e.g., 22:00 UTC), including 12, 24, 36, 48, 60, and 72 hours in red, orange, green, blue, magenta, and purple, respectively.

Fig. S7 Trajectories from FLEXPART-WRF in NCP for episodes of Type II, with different colors indicating the number of hours prior to the end of the event (e.g., 22:00 UTC), including 12, 24, 36, 48, 60, and 72 hours in red, orange, green, blue, magenta, and purple, respectively.

Table S1 Model configuration of WRF.

WRF configuration	Scheme
Microphysics	Morrison microphysics scheme (Morrison et al., 2009)
Land surface option	Unified Noah land surface model (Chen and Dudhia, 2001)
Longwave and shortwave radiation	Rapid Radiation Transfer Model Global (RRTMG) (Morcrette et al., 2008; Iacono et al., 2008)
Cumulus parameterization scheme	GrellFreitas cumulus parameterization scheme (Grell and Freitas, 2014)
Planetary boundary layer scheme	YSU (Hong et al., 2006)

Table S2 The evaluation of daily meteorological parameters, including air temperature at 2 m (T_2), specific humidity at 2 m (Q_2), wind speed (WS_{10}), and direction (WD_{10}) at 10 m from WRF model simulation and NCDC observation.

	Model evaluation				**Benchmarks (Emery and Tai, 2001)**			
	T_2	**Q_2**	**WD_{10}**	**WS_{10}**	**T_2**	**Q_2**	**WD_{10}**	**WS_{10}**
Bias	-0.28	0.01	0.03	0.85	$\leq \pm 0.5$	$\leq \pm 1$	$\leq \pm 10$	$\leq \pm 0.5$
Gross	1.97	0.01	45.98	/	≤ 2	≤ 2	≤ 30	/
RMSE	/	/	/	1.62	/	/	/	≤ 2

Table S3 The total number of polluted days exceedance in SWLY during winters in 2014-2019.

	75-150 μg m^{-3}	150-250 μg m^{-3}	greater than 250 μg m^{-3}	total[a]
seesaw patterns	98	22	1	121
stagnation	105	32	1	138
other	118	10	0	128
total[b]	321	64	2	387

a indicates the total number of polluted days due to seesaw patterns, stagnation days, and others; b indicates the total number of days in three categories.

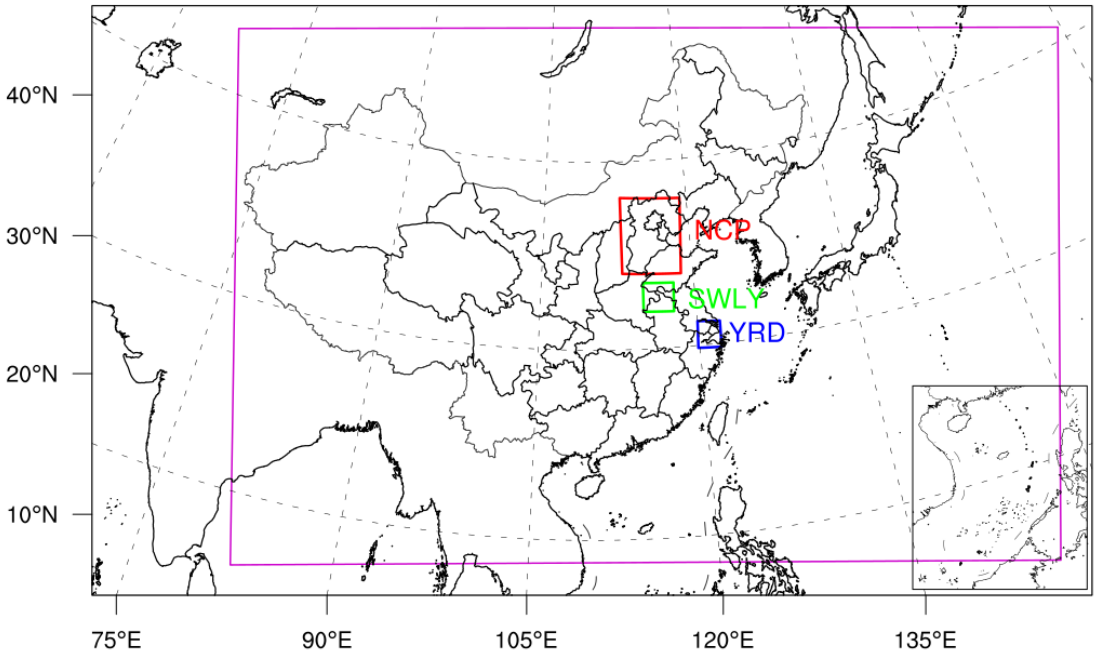

Fig. S1 The simulation domains of WRF (black square), CMAQ (magenta square) and the regions of NCP (red square), SWLY (green square), and YRD (blue square) used for the analysis.

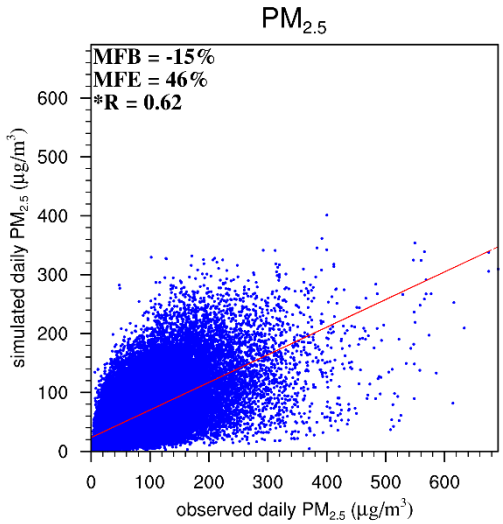

Fig. S2 Scatter plot of simulated and observational daily mean $PM_{2.5}$ over three regions (NCP, SWLY, and YRD) from 2014 to 2019. The linear regression is marked in red line. The statistical parameters are also shown on the top left, including mean fractional bias (MFB), mean fractional error percent (MFE), and correlation coefficient (R), with the asterisk on the top left of R indicating statistical significance ($P < 0.05$).

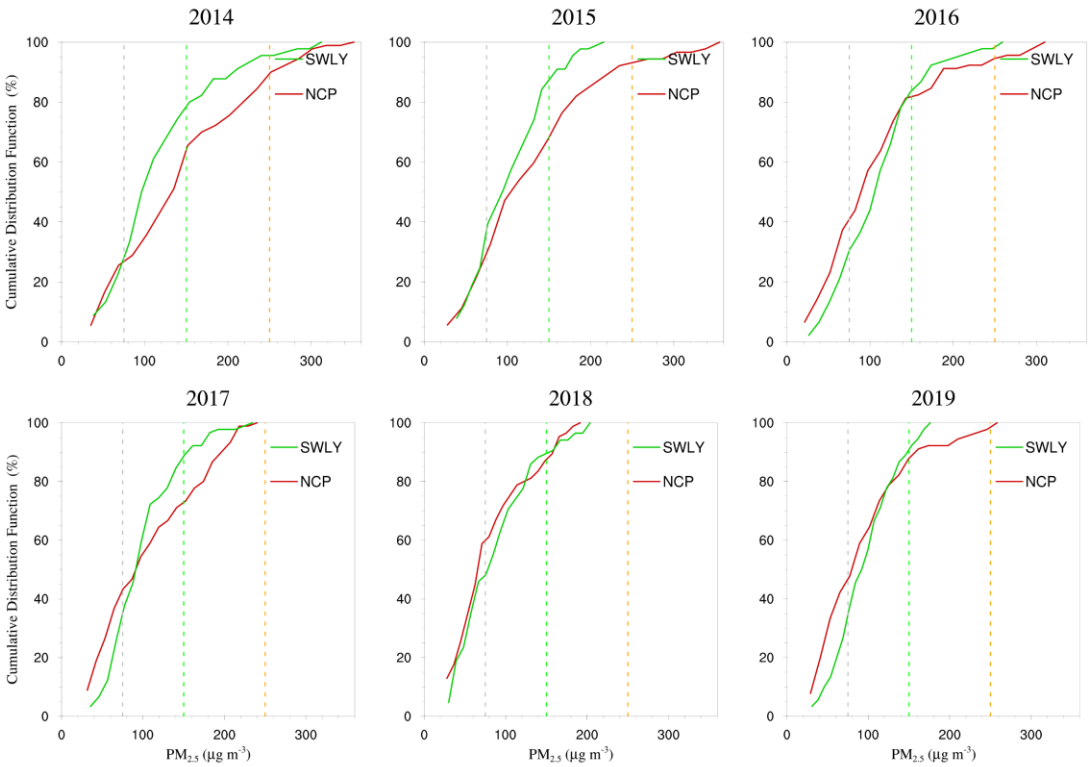

Fig. S3 The cumulative distribution function of observational daily $PM_{2.5}$ in wintertime of SWLY in 2014-2019. The grey, green and orange dotted lines implies 75, 150, and 250 μg m^{-3} of $PM_{2.5}$ concentrations, respectively.

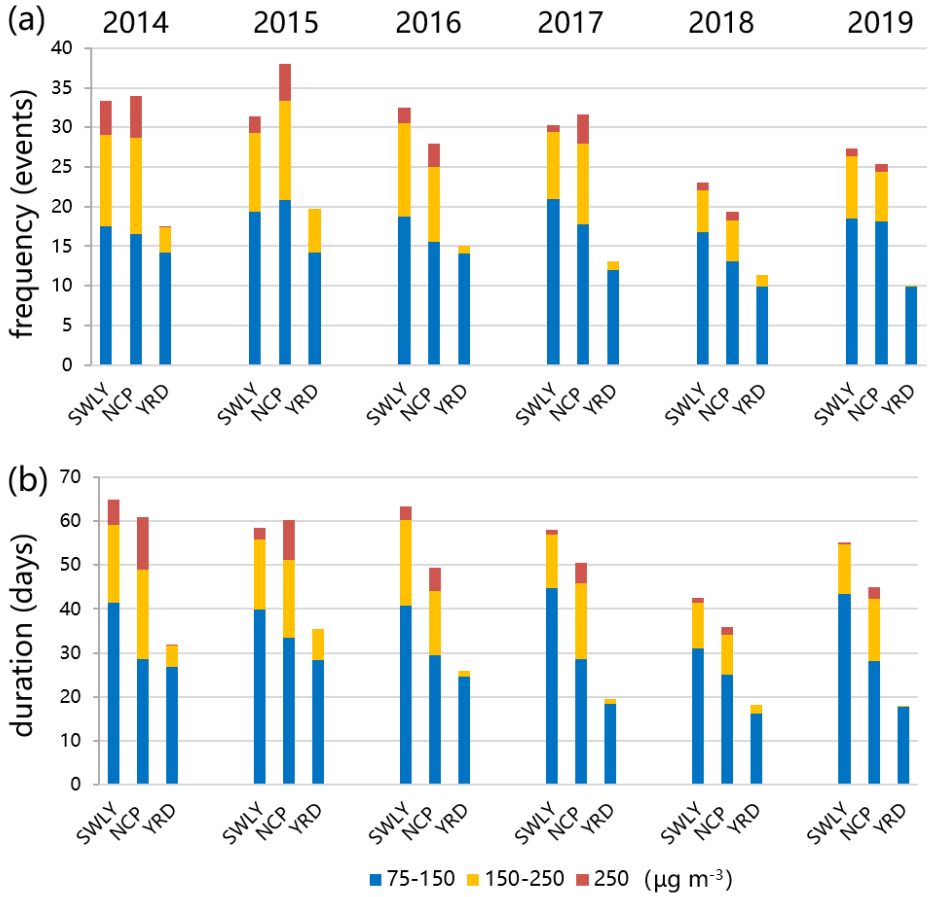

Fig. S4 The regional mean total frequency (a) and duration (b) of observational $PM_{2.5}$ for three categories (I: 75-150 μg m^{-3} II: 150-250 μg m^{-3}, III: greater than 250 μg m^{-3}) over SWLY, NCP and YRD in winter during 2014-2019.

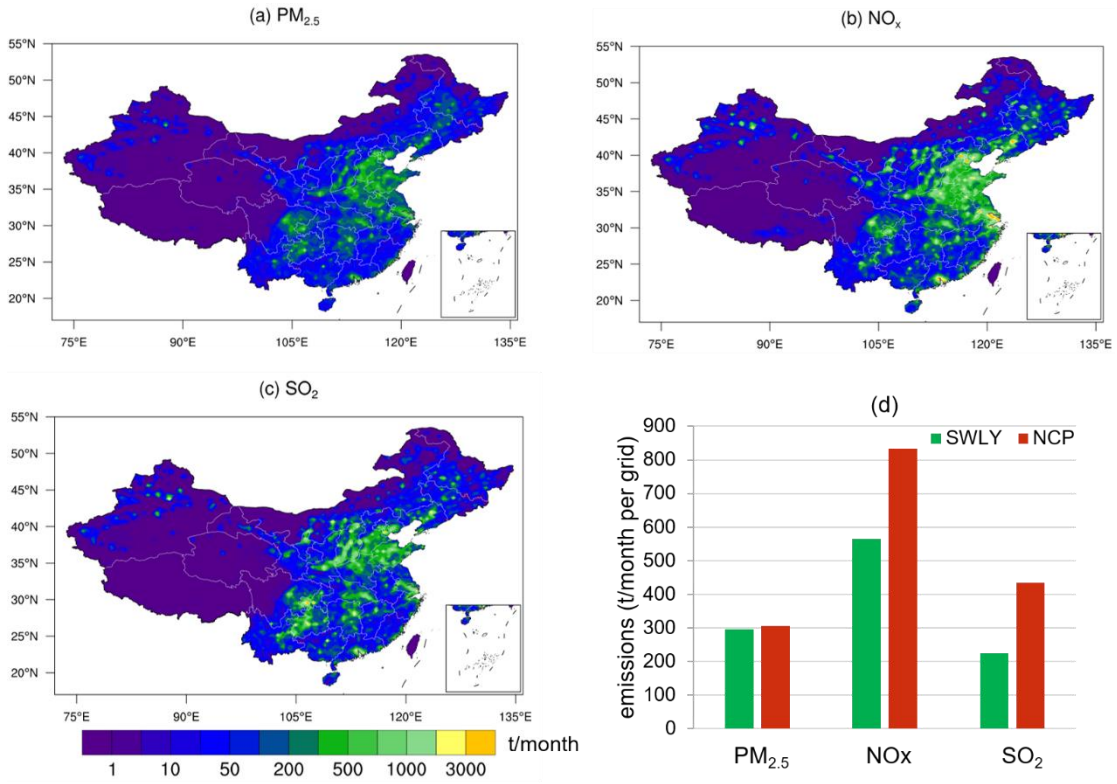

Fig. S5 (a)-(c): Monthly average emissions of (t/month) from MEIC emission inventory in winter 2016; (d) The monthly average emissions of $PM_{2.5}$, NO_X, and SO_2 derived from MEIC in SWLY and NCP in winter 2016.

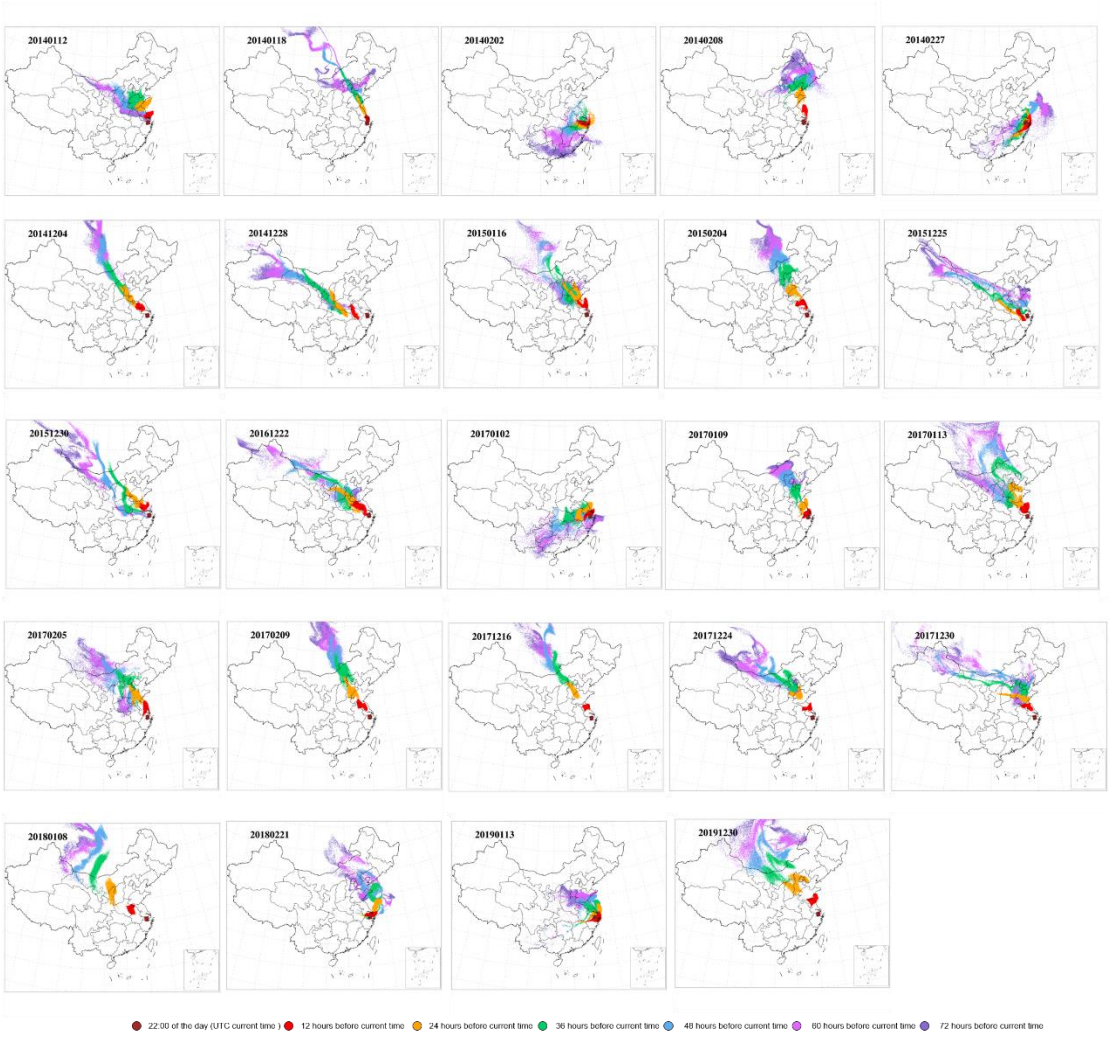

Fig. S6 Trajectories from FLEXPART-WRF in YRD for episodes of Type I, with different colors indicating the number of hours prior to the end of the event (e.g., 22:00 UTC), including 12, 24, 36, 48, 60, and 72 hours in red, orange, green, blue, magenta, and purple, respectively.

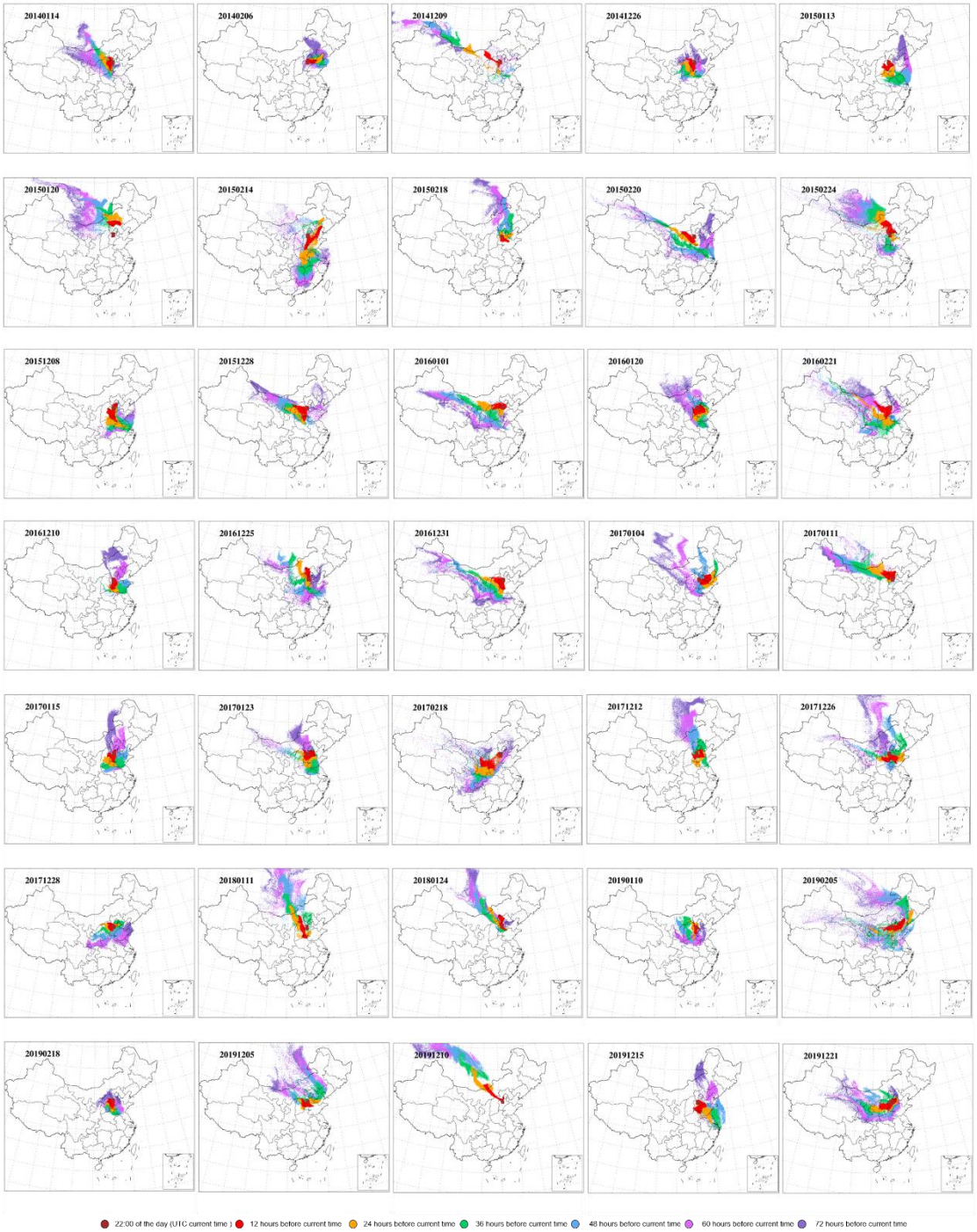

Fig. S7 Trajectories from FLEXPART-WRF in NCP for episodes of Type II, with different colors indicating the number of hours prior to the end of the event (e.g., 22:00 UTC), including 12, 24, 36, 48, 60, and 72 hours in red, orange, green, blue, magenta, and purple, respectively.

Reference

Chen, F. and Dudhia, J.: Coupling an advanced land surface-hydrology model with the Penn State-NCAR MM5 modeling system. Part I: Model implementation and sensitivity, Mon. Weather Rev., 129, 569-585, 10.1175/1520-0493(2001)129<0569:Caalsh>2.0.Co;2, 2001.

Emery, C. and Tai, E.: Enhanced Meteorological Modeling and Performance Evaluation for Two Texas Ozone Episodes, prepared for the Texas Natural Resource Conservation Commission, ENVIRON International Corp, https://api.semanticscholar.org/CorpusID:127579774, 2001.

Grell, G. A. and Freitas, S. R.: A scale and aerosol aware stochastic convective parameterization for weather and air quality modeling, Atmos. Chem. Phys., 14, 5233-5250, 10.5194/acp-14-5233-2014, 2014.

Hong, S. Y., Noh, Y., and Dudhia, J.: A new vertical diffusion package with an explicit treatment of entrainment processes, Mon. Weather Rev., 134, 2318-2341, 10.1175/mwr3199.1, 2006.

Iacono, M. J., Delamere, J. S., Mlawer, E. J., Shephard, M. W., Clough, S. A., and Collins, W. D.: Radiative forcing by long-lived greenhouse gases: Calculations with the AER radiative transfer models, J. Geophys. Res. Atmos., 113, 10.1029/2008jd009944, 2008.

Morcrette, J.-J., Barker, H. W., Cole, J. N. S., Iacono, M. J., and Pincus, R.: Impact of a New Radiation Package, McRad, in the ECMWF Integrated Forecasting System, Mon. Weather Rev., 136, 4773-4798, 10.1175/2008mwr2363.1, 2008.

Morrison, H., Thompson, G., and Tatarskii, V.: Impact of Cloud Microphysics on the Development of Trailing Stratiform Precipitation in a Simulated Squall Line: Comparison of One- and Two-Moment Schemes, Mon. Weather Rev., 137, 991-1007, 10.1175/2008mwr2556.1, 2009.